Estimating winter balance and its uncertainty from direct measurements of snow depth and density on alpine glaciers

ALEXANDRA PULWICKI,[1] GWENN E. FLOWERS,[1] VALENTINA RADIĆ,[2] DEREK BINGHAM[3]

[1]*Department of Earth Sciences, Simon Fraser University, Burnaby, BC, Canada*
[2]*Department of Earth, Ocean and Atmospheric Sciences, University of British Columbia, Vancouver, BC, Canada*
[3]*Department of Statistics and Actuarial Science, Simon Fraser University, Burnaby, BC, Canada*
Correspondence: Alexandra Pulwicki <apulwick@sfu.ca>

ABSTRACT. Accurately estimating winter surface mass balance on glaciers is central to assessing glacier health and predicting glacier run-off. However, measuring and modelling snow distribution is inherently difficult in mountainous terrain. Here, we explore rigorous statistical methods of estimating winter balance and its uncertainty from multiscale measurements of snow depth and density. In May 2016, we collected over 9000 manual measurements of snow depth across three glaciers in the St. Elias Mountains, Yukon, Canada. Linear regression, combined with cross-validation and Bayesian model averaging, as well as ordinary kriging are used to interpolate point-scale values to glacier-wide estimates of winter balance. Elevation and a wind-redistribution parameter exhibit the highest correlations with winter balance, but the relationship varies considerably between glaciers. A Monte Carlo analysis reveals that the interpolation itself introduces more uncertainty than the assignment of snow density or the representation of grid-scale variability. For our study glaciers, the winter balance uncertainty from all assessed sources ranges from 0.03 to 0.15 m w.e. (5–39%). Despite the challenges associated with estimating winter balance, our results are consistent with a regional-scale winter-balance gradient.

KEYWORDS: winter balance, accumulation, glacier mass balance, snow, St. Elias Mountains, Yukon

1. INTRODUCTION

Winter surface mass balance, or 'winter balance', is the net accumulation and ablation of snow over the winter season (Cogley and others, 2011), which constitutes glacier mass input. Winter balance (B_w) is half of the seasonally resolved mass balance, initializes summer ablation conditions and must be estimated to simulate energy and mass exchange between the land and atmosphere (e.g. Hock, 2005; Réveillet and others, 2016). Effectively representing the spatial distribution of snow on glaciers is also central to monitoring surface run-off and its downstream effects (e.g. Clark and others, 2011).

Winter balance is notoriously difficult to estimate (e.g. Dadić and others, 2010; Cogley and others, 2011). Snow distribution in alpine regions is highly variable with short correlation length scales (e.g. Anderton and others, 2004; Egli and others, 2011; Grünewald and others, 2010; Helbig and van Herwijnen, 2017; López-Moreno and others, 2011, 2013; Machguth and others, 2006; Marshall and others, 2006) and is influenced by dynamic interactions between the atmosphere and complex topography, operating on multiple spatial and temporal scales (e.g. Barry, 1992; Liston and Elder, 2006; Clark and others, 2011; Scipión and others, 2013). Simultaneously extensive, high resolution and accurate snow distribution measurements on glaciers are therefore difficult to acquire (e.g. Cogley and others, 2011; McGrath and others, 2015) and obtaining such measurements is further complicated by the inaccessibility of many glacierized regions during the winter. Use of physically based models to estimate winter balance is computationally intensive and requires detailed meteorological data to drive the models (Dadić and others, 2010). As a result, there is significant uncertainty in estimates of winter balance, thus limiting the ability of models to represent current and projected glacier conditions.

Studies that have focused on obtaining detailed estimates of B_w have used a wide range of observational techniques, including direct measurement of snow depth and density (e.g. Cullen and others, 2017), lidar or photogrammetry (e.g. Sold and others, 2013) and ground-penetrating radar (e.g. Machguth and others, 2006; Gusmeroli and others, 2014; McGrath and others, 2015). Spatial coverage of direct measurements is generally limited and often comprises an elevation transect along the glacier centreline (e.g. Kaser and others, 2003). Measurements are typically interpolated using linear regression on only a few topographic parameters (e.g. MacDougall and Flowers, 2011), with elevation being the most common. Other established techniques include hand contouring (e.g. Tangborn and others, 1975), kriging (e.g. Hock and Jensen, 1999) and attributing measured winter balance values to elevation bands (e.g. Thibert and others, 2008). Physical snow models have been used to estimate spatial patterns of winter balance (e.g. Mott and others, 2008; Schuler and others, 2008; Dadić and others, 2010), but the availability of the required meteorological data generally prohibits their widespread application. Error analysis is rarely undertaken and few studies have thoroughly investigated uncertainty in spatially distributed estimates of winter balance (e.g. Schuler and others, 2008).

More sophisticated snow-survey designs and statistical models of snow distribution are widely used in the field of snow science. Surveys described in the snow science literature are generally spatially extensive and designed to

measure snow depth and density throughout a basin, ensuring that all terrain types are sampled. A wide array of measurement interpolation methods are used, including linear (e.g. López-Moreno and others, 2010) and non-linear regressions (e.g. Molotch and others, 2005) that include numerous terrain parameters, as well as geospatial interpolation (e.g. Erxleben and others, 2002; Cullen and others, 2017) including various forms of kriging. Different interpolation methods are also combined; for example, regression kriging (see Supplementary Material) adds kriged residuals to a field obtained with linear regression (e.g. Balk and Elder, 2000). Physical snow models such as SnowTran-3D (Liston and Sturm, 1998), Alpine3D (Lehning and others, 2006) and SnowDrift3D (Schneiderbauer and Prokop, 2011) are widely used, and errors in estimating snow distribution have been examined from theoretical (e.g. Trujillo and Lehning, 2015) and applied perspectives (e.g. Turcan and Loijens, 1975; Woo and Marsh, 1978; Deems and Painter, 2006).

The goals of this study are to (1) critically examine methods of converting direct snow depth and density measurements to distributed estimates of winter balance; and (2) identify sources of uncertainty, evaluate their magnitude and assess their combined contribution to uncertainty in glacier-wide winter balance. We focus on commonly applied, low-complexity methods of measuring and estimating winter balance in the interest of making our results broadly applicable.

2. STUDY SITE

The St. Elias Mountains (Fig. 1a) rise sharply from the Pacific Ocean, creating a significant climatic gradient between coastal maritime conditions, generated by Aleutian–Gulf of Alaska low-pressure systems, and interior continental conditions, driven by the Yukon–Mackenzie high-pressure system (Taylor-Barge, 1969). The boundary between the two climatic zones is generally aligned with the divide between the Hubbard and Kaskawulsh Glaciers, ~130 km from the coast. Research on snow distribution and glacier mass balance in this area is limited. A series of research programs, including Project 'Snow Cornice' and the Icefield Ranges Research Project, were operational in the 1950s and 60s (Wood, 1948; Danby and others, 2003) and in the last 30 years, there have been a few long-term studies on selected alpine glaciers (e.g. Clarke, 2014), as well as several regional studies of glacier mass balance and dynamics (e.g. Arendt and others, 2008; Berthier and others, 2010; Burgess and others, 2013; Waechter and others, 2015).

We carried out winter-balance surveys on three unnamed glaciers in the Donjek Range of the St. Elias Mountains. The Donjek Range is located ~40 km to the east of the regional mountain divide and has an area of $\sim 30 \times 30$ km^2. Glacier 4, Glacier 2 and Glacier 13 (labelling adopted from Crompton and Flowers (2016)) are located along a southwest–northeast transect through the range (Fig. 1b, Table 1). These small alpine glaciers are generally oriented southeast–northwest, with Glacier 4 having a predominantly southeast aspect and Glaciers 2 and 13 having generally northwest aspects. The glaciers are situated in valleys with steep walls and have simple geometries. Based on a detailed study of Glacier 2 (Wilson and others, 2013) and related theoretical modelling (Wilson and Flowers, 2013), we suspect all of the study glaciers to be polythermal.

3 METHODS

Estimating glacier-wide winter balance (B_w) involves transforming measurements of snow depth and density into values of winter balance distributed across a defined grid (b_w). We do this in four steps. (1) Obtain direct measurements of snow depth and density in the field. (2) Assign density values to all depth-measurement locations to calculate point-scale values of b_w at each location. Winter balance, measured in units of m w.e., can be estimated as the product of snow depth and depth-averaged density. (3) Average all point-scale values of b_w within each gridcell of a DEM to obtain the gridcell-averaged b_w. (4) Interpolate and extrapolate these gridcell-averaged b_w values to obtain estimates of b_w in each gridcell across the domain. B_w is then calculated by taking the average of all gridcell-averaged b_w values for each glacier. For brevity, we refer to these four steps as (1) field measurements, (2) density assignment, (3) gridcell-averaged b_w and (4) distributed b_w. Detailed methodology for each step is outlined below. We use the SPIRIT SPOT-5 DEM (40 m × 40 m) from 2005 (Korona and others, 2009) throughout this study.

3.1. Field measurements

Our sampling campaign involved four people and occurred between 5 and 15 May 2016, which falls within the period of historical peak snow accumulation in southwestern Yukon (Yukon Snow Survey Bulletin and Water Supply Forecast, 1 May 2016). Snow depth is generally accepted to be more variable than density (Elder and others, 1991; Clark and others, 2011; López-Moreno and others, 2013) so we chose a sampling design that resulted in a high ratio (~55:1) of snow depth to density measurements. In total, we collected more than 9000 snow-depth measurements and more than 100 density measurements throughout the study area (Table 1).

During the field campaign, there were two small accumulation events. The first, on 6 May 2016, also involved high winds so accumulation could not be determined. The second, on 10 May 2016, resulted in 0.01 m w.e. accumulation measured at one location on Glacier 2. Assuming both accumulation events contributed a uniform 0.01 m w.e. accumulation to all study glaciers then our survey did not capture ~3 and ~2% of estimated B_w on Glaciers 4 and 2, respectively. We, therefore, assume that these accumulation events were negligible and apply no correction. Positive temperatures and clear skies occurred between 11 and 16 May 2016, which we suspect resulted in melt occurring on Glacier 13. The snow in the lower part of the ablation area of Glacier 13 was isothermal and showed clear signs of melt and metamorphosis. The total amount of melt during the study period was estimated using a degree-day model and found to be small (≤0.01 m w.e., see Supplementary Material) so no corrections were made.

3.1.1. Sampling design

The snow surveys were designed to capture variability in snow depth at regional, basin, gridcell and point scales (Clark and others, 2011). To capture variability at the regional scale, we chose three glaciers along a transect aligned with the dominant precipitation gradient (Fig. 1b) (Taylor-Barge, 1969). To account for basin-scale variability, snow depth was measured along linear and curvilinear transects on each glacier (Fig. 1c) with a sample spacing of
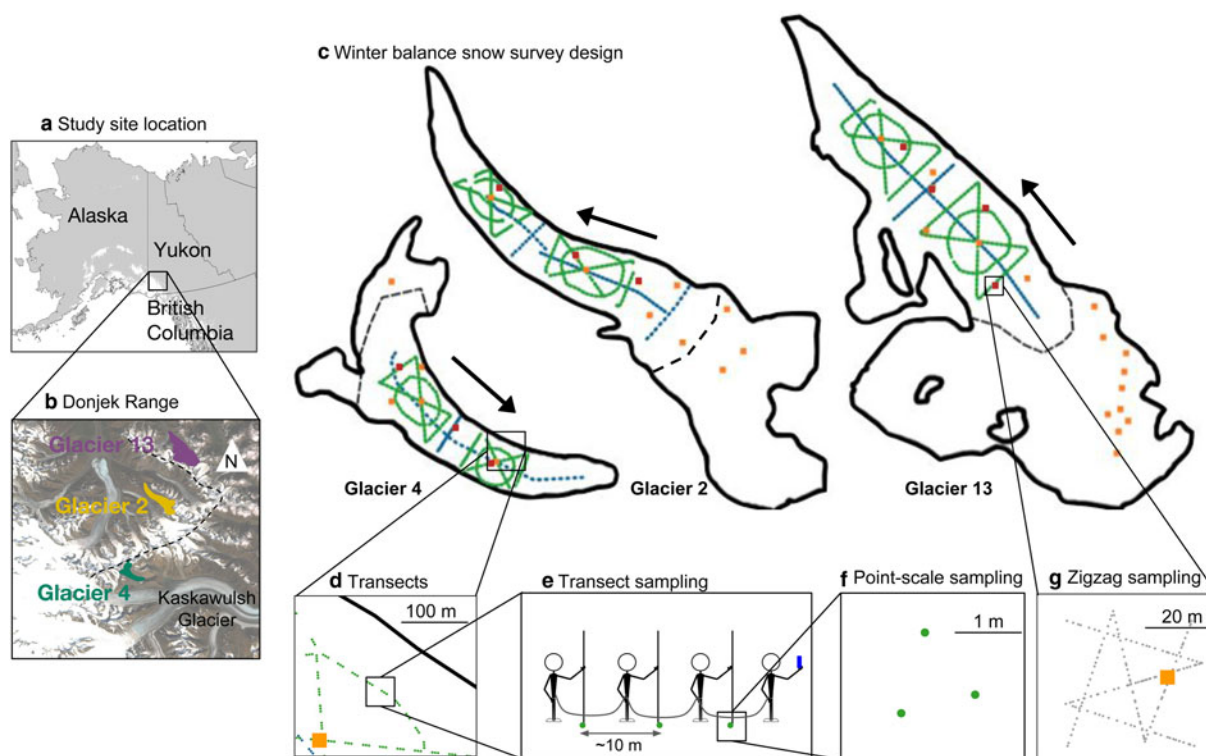
Fig. 1. Study area location and sampling design for Glaciers 4, 2 and 13. (a) Study region in the Donjek Range of the St. Elias Mountains of Yukon, Canada. (b) Study glaciers located along a southwest–northeast transect through the Donjek Range. The local topographic divide is shown as a dashed line. Imagery from Landsat 8 (5 September 2013, data available from the US Geological Survey). (c) Details of the snow-survey sampling design, with centreline and transverse transects (blue dots), hourglass and circle designs (green dots) and locations of snow density measurements (orange squares). Arrows indicate ice-flow directions. Approximate location of ELA on each glacier is shown as a black dashed line. (d) Close up of linear and curvilinear transects. (e) Configuration of navigator and observers. (f) Point-scale snow-depth sampling. (g) Linear-random snow-depth measurements in 'zigzag' design (red dots) with one density measurement (orange square) per zigzag.

10–60 m (Fig. 1d). Sample spacing was constrained by protocols for safe glacier travel, while survey scope was constrained by the need to complete all surveys within the period of peak accumulation. We selected centreline and transverse transects as the most commonly used survey designs in winter-balance studies (e.g. Kaser and others, 2003; Machguth and others, 2006) as well as an hourglass pattern with an inscribed circle, which allows for sampling in multiple directions and easy travel (personal communication from C. Parr, 2016). To capture variability at the grid scale, we densely sampled up to four gridcells on each glacier using a linear-random sampling design (Shea and Jamieson, 2010), which we term a 'zigzag'. To capture point-scale variability, each observer made 3–4 depth measurements within ~1 m (Fig. 1f) at each transect measurement location.

3.1.2. Snow depth: transects
While roped-up for glacier travel with fixed distances between observers, the lead observer used a single-frequency GPS unit (Garmin GPSMAP 64s) to navigate between predefined transect measurement locations (Fig. 1e). The remaining three observers used 3.2 m graduated aluminum avalanche probes to make snow-depth measurements (Kinar and Pomeroy, 2015). The locations of each set of depth measurements, made by the second, third and fourth observers, are estimated using the recorded location of the first observer, the approximate distance between observers and the direction of travel. The 3–4 point-scale depth measurements are averaged to obtain a single depth measurement at each transect measurement location. When considering variability at the point scale as a source of uncertainty in snow depth measurements, we find that the mean standard deviation of point-scale snow depth measurements is <7% of the mean snow depth for all study glaciers.

Snow-depth sampling was concentrated in the ablation area to ensure that only snow from the current accumulation season was measured. The boundary between snow and firn in the accumulation area can be difficult to detect and often misinterpreted, especially when using an avalanche probe

Table 1. Physical characteristics of the study glaciers

	Location		Elevation (m a.s.l)			Slope (∘)	Area (km^2)
	UTM Zone 7		Mean	Range	ELA	Mean	
Glacier 4	59 5470 E	674 0730 N	2344	1958–2809	~2500	12.8	3.8
Glacier 2	60 1160 E	675 3785 N	2495	1899–3103	~2500	13.0	7.0
Glacier 13	60 4602 E	676 3400 N	2428	1923–3067	~2380	13.4	12.6

(Grünewald and others, 2010; Sold and others, 2013). We intended to use a firn corer to measure winter balance in the accumulation area, but cold snow combined with positive air temperatures led to cores being unrecoverable. Successful snow-depth measurements within the accumulation area were made either in snow pits or using a Federal Sampler (described below) to unambiguously identify the snow/firn transition.

3.1.3. Snow depth: zigzags
We measured depth at random intervals of 0.3–3.0 m along two 'Z'-shaped patterns (Shea and Jamieson, 2010), resulting in 135–191 measurements per zigzag, within three 40 m × 40 m gridcells (Fig. 1g) per glacier. Random intervals were computer-generated from a uniform distribution in sufficient numbers that each survey was unique. Zigzag locations were randomly chosen within the upper, middle and lower regions of the ablation area of each glacier. Extra time in the field allowed us to measure a fourth zigzag on Glacier 13 in the central ablation area at ~2200 m a.s.l.

3.1.4. Snow density
Snow density was measured using a Snowmetrics wedge cutter in three snow pits (SP) on each glacier. Within the snow pits, we measured a vertical density profile (in 10 cm increments) with the 5 cm × 5 cm × 10 cm wedge-shaped cutter (250 cm^3) and a Presola 1000 g spring scale (e.g. Gray and Male, 1981; Fierz and others, 2009; Kinar and Pomeroy, 2015). Wedge-cutter error is ~ ±6% (e.g. Proksch and others, 2016; Carroll, 1977). Uncertainty in estimating density from SP measurements also stems from incorrect assignment of density to layers that cannot be sampled (e.g. ice lenses and hard layers). We attempt to quantify this uncertainty by varying estimated ice-layer thickness by ±1 cm (≤100%) of the recorded thickness, ice layer density between 700 and 900 kg m^{-3} and the density of layers identified as being too hard to sample (but not ice) between 600 and 700 kg m^{-3}. When considering all three sources of uncertainty, the range of integrated density values is always <15% of the reference density. Depth-averaged densities for shallow pits (<50 cm) that contain ice lenses are particularly sensitive to changes in prescribed density and ice-lens thickness.

While snow pits provide the most accurate measure of snow density, digging and sampling a snow pit is time and labour intensive. Therefore, a Geo Scientific Ltd. metric Federal Sampler (FS) (Clyde, 1932) with a 3.2–3.8 cm diameter sampling tube, which directly measures depth-integrated snow water equivalent, was used to augment the SP measurements. A minimum of three FS measurements were taken at each of 7–19 locations on each glacier and an additional

eight FS measurements were co-located with two SP profiles for each glacier. Measurements for which the snow core length inside the sampling tube was <90% of the snow depth were discarded. Densities at each measurement location (eight at each SP, three elsewhere) were then averaged, with the standard deviation taken to represent the uncertainty. The mean standard deviation of FS-derived density was ≤4% of the mean density for all glaciers.

3.2. Density assignment
Measured snow density must be interpolated or extrapolated to estimate point-scale b_w at each snow-depth sampling location. We employ four commonly used methods to interpolate and extrapolate density (Table 2): (1) calculate mean density over an entire mountain range (e.g. Cullen and others, 2017), (2) calculate mean density for each glacier (e.g. Elder and others, 1991; McGrath and others, 2015), (3) linear regression of density on elevation for each glacier (e.g. Elder and others, 1998; Molotch and others, 2005) and (4) calculate mean density using inverse-distance weighting (e.g. Molotch and others, 2005) for each glacier. Densities derived from SP and FS measurements are treated separately, for reasons explained below, resulting in eight possible methods of assigning density.

3.3. Gridcell-averaged winter balance
We average one to six (mean of 2.1 measurements) point-scale values of b_w within each DEM gridcell to obtain the gridcell-averaged b_w. The locations of individual measurements have uncertainty due to the error in the horizontal position given by the GPS unit and the estimation of observer location based on the recorded GPS positions of the navigator. This location uncertainty could result in the incorrect assignment of a point-scale b_w measurement to a particular gridcell. However, this source of error is not further investigated because we assume that the uncertainty resulting from incorrect locations of point-scale b_w values is captured in the uncertainty derived from zigzag measurements, as described below. Error due to having multiple observers is also evaluated by conducting an analysis of variance (ANOVA) of snow-depth measurements along a transect (amounting to 23 hypothesis tests, one for each transect) and testing for differences between observers. We find no significant differences between snow-depth measurements made by observers along any transect ($p > 0.05$), with the exception of the first transect on Glacier 4 (51 measurements), where snow-depth measurements collected by one observer were, on average, greater than snow-depth measurements taken by the other two observers ($p < 0.01$). Since this was the first transect and the only one to show

Table 2. Details of the May 2016 winter-balance survey, including number of snow-depth measurement locations along transects (n_T), total length of transects (d_T), number of combined snow pit and Federal Sampler density measurement locations (n_p), number of zigzag surveys (n_{zz}), number (as percent of total number of gridcells and of the number of gridcells in the ablation area) of gridcells sampled (n_s) and the elevation range (as percent of total elevation range and of ablation-area elevation range)

	Date	n_T	d_T (km)	n_p	n_{zz}	n_s	Elevation range (m a.s.l.)
Glacier 4	4–7 May 2016	649	13.1	7	3	295 (12%, 21%)	2015–2539 (62%, 97%)
Glacier 2	8–11 May 2016	762	13.6	7	3	353 (8%, 14%)	2151–2541 (32%, 47%)
Glacier 13	12–15 May 2016	941	18.1	19	4	468 (6%, 14%)	2054–2574 (45%, 62%)

differences by observer, this difference can be considered an anomaly. We conclude that observer bias is not an important effect in this study and therefore apply no observer corrections to the data.

3.4. Distributed winter balance

Gridcell-averaged values of b_w are interpolated and extrapolated across each glacier using linear regression (LR) and ordinary kriging (OK). The LR relates gridcell-averaged b_w to various topographic parameters. We use this method because it is simple and has precedent for success (e.g. McGrath and others, 2015). Instead of a standard LR, however, we use cross-validation implemented in such a way as to prevent data overfitting, and employ model averaging to allow for all combinations of the chosen topographic parameters. To compliment the LR approach, we also use a Gaussian Process regression with a constant mean and specified covariance, hereafter referred to as OK, to interpolate and extrapolate gridcell-averaged b_w. This approach is an interpolation method free of physical interpretation beyond the premise of spatial correlation in the data (e.g. Hock and Jensen, 1999; Rasmussen and Williams, 2006).

3.4.1. Linear regression

Commonly defined topographic parameters are selected as regressors within the LR. As in McGrath and others (2015) we include elevation, slope, aspect, curvature, 'northness' and a wind-redistribution parameter (Sx from Winstral and others (2002)); we add distance-from-centreline as an additional parameter. Topographic parameters are standardized for use in the LR. The goal of the LR is to obtain a set of fitted regression coefficients (β) that correspond to each topographic parameter (regressor) and to a model intercept. For details on data and methods used to estimate the topographic parameters see the Supplementary Material and Pulwicki (2017). Our sampling design ensured that the ranges of topographic parameters associated with our measurement locations represent more than 70% of the total area of each glacier (except elevation on Glacier 2, where our measurements captured only 50%).

We use a combination of cross-validation and model averaging to avoid overfitting the data, to account for uncertainty in the selected predictors and to maximize the model's predictive ability (Madigan and Raftery, 1994; Kohavi, 1995). Since there are seven predictors, there are 2^7 possible subsets of predictors, or equivalently, models.

For a given model, we randomly select 1000 subsets of the data (where each subset includes ~2/3 of the data) and fit a multiple LR using least squares (implemented in MATLAB), thus obtaining 1000 sets of β. Distributed b_w is then calculated by multiplying the topographic parameters by their corresponding regression coefficients for all DEM gridcells. We use the remaining data (~1/3 of the values) to calculate a RMSE between the estimated and observed b_w at the measurement locations. From the 1000 sets of β values, we select the set that results in the lowest RMSE. This set of β has the greatest predictive ability for a particular linear combination of topographic parameters. The procedure above is repeated for each of the models, giving the best β set for each of the 2^7 models.

With the β's in hand, we move on to prediction of distributed winter balance. To do so, we use Bayesian model averaging. We weight the models according to their relative predictive success, as assessed by the value of the Bayesian Information Criterion (BIC) (Burnham and Anderson, 2004). BIC penalizes more complex models, which reduces the risk of overfitting. The final value of each β is then the weighted sum of β from all models. The final estimate of distributed b_w is calculated by multiplying the topographic parameters by the final set of β for all DEM gridcells.

3.4.2. Ordinary kriging

Kriging is a method of estimating dependent variables at unsampled locations by using the spatial correlation of measured values to find a set of optimal weights (Davis and Sampson, 1986; Li and Heap, 2008). Kriging assumes spatial correlation between the dependent variables at the sampling locations distributed across a surface and then applies the correlation to interpolate between these locations. Many forms of kriging have been developed to accommodate different data types (e.g. Li and Heap, 2008, and sources therein). OK is the simplest form of kriging in cases where the mean of the estimated field is unknown. Unlike LR, OK is neither useful for generating hypotheses to explain the physical controls on snow distribution, nor can it be used to estimate winter balance on unmeasured glaciers. However, we chose to use OK because it does not require external inputs and is, therefore, a means of obtaining B_w that is free of physical interpretation beyond the information contained in the covariance matrix.

The OK model can be written $y(s) = \mu + z(s) + e$, where μ is the mean and e is independent white noise with standard deviation σ_e (also known as the nugget) that captures the sampling error as well as spatial variation at distances less than those observed in the sampling design (Li and Heap, 2008); $z(s)$ follows a mean-zero normal distribution with standard deviation σ_z. The covariance of observations at spatial locations s and s' is written as $Cov(z(s), z(s')) = \sigma_z^2 r(s, s')$ and r is a specified correlation model. We use the DiceKriging package in R (Roustant and others, 2012) to implement OK. For our application, we employ an isotropic Matérn correlation model with shape parameter $v = 5/2$ (see Rasmussen and Williams, 2006). This specification implies a fairly smooth response surface (twice differentiable) and is used in many applications (e.g. Stein, 1999). The model parameters, μ, σ_e, σ_z and range parameter for the Matérn correlation function, are estimated using maximum likelihood. There is no closed form solution for these parameter estimates so they are found numerically. To ensure stability of the maximum likelihood solution, we use 500 random restarts of the DiceKringing package (each with a different initial value of the parameters).

3.5. Uncertainty analysis using a Monte Carlo approach

Three sources of uncertainty are considered separately: the uncertainty due to (1) grid-scale variability of b_w (σ_{GS}), (2) the assignment of snow density (σ_ρ) and (3) interpolating and extrapolating gridcell-averaged values of b_w (σ_{INT}). To quantify the combined uncertainty due to grid-scale variability, the method of density assignment and interpolation uncertainty on estimates of B_w, we conduct a Monte Carlo analysis that uses repeated random sampling of input variables to calculate a distribution of output variables

(Metropolis and Ulam, 1949). We repeat the random sampling process 1000 times, resulting in a distribution of values of B_w based on uncertainties associated with the four steps we implement to derive B_w from distributed snow-depth and density measurements. Individual sources of uncertainty are propagated through the conversion of snow depth and density measurements to B_w. Finally, the combined effect of all three sources of uncertainty on B_w is quantified. We use the standard deviation of the distribution of B_w as a useful metric of B_w uncertainty. Density assignment uncertainty is calculated as the standard deviation of the eight resulting values of B_w. To investigate the spatial patterns in b_w uncertainty, we calculate a combined uncertainty, which is equal to the square root of the summed variance of distributed b_w that arises from σ_{GS}, σ_ρ and σ_{INT}. See Supplementary Material (Figs. S5 and S6) for plots of standard deviation of distributed b_w arising from individual sources of uncertainty.

3.5.1. Grid-scale uncertainty (σ_{GS})
We make use of the zigzag surveys to quantify the true variability of b_w at the grid scale. Our limited data do not permit a spatially-resolved assessment of grid-scale uncertainty, so we characterize this uncertainty as uniform across each glacier and represent it by a normal distribution. The distribution is centred at zero and has a standard deviation equal to the mean standard deviation of all zigzag measurements for each glacier. For each iteration of the Monte Carlo, b_w values are randomly chosen from the distribution and added to the values of gridcell-averaged b_w. These perturbed gridcell-averaged values of b_w are then used in the interpolation. We represent uncertainty in B_w due to grid-scale uncertainty (σ_{GS}) as the standard deviation of the resulting distribution of B_w estimates.

3.5.2. Density assignment uncertainty (σ_ρ)
We incorporate uncertainty due to the method of density assignment by carrying forward all eight density interpolation methods (Table 3) when estimating B_w. By choosing to retain even the least plausible options, as well as the questionable FS data (see below), this approach results in a generous assessment of uncertainty. We represent the B_w uncertainty due to density assignment uncertainty (σ_ρ) as the standard deviation of B_w estimates calculated using each density assignment method.

3.5.3 Interpolation uncertainty (σ_{INT})
We represent the uncertainty due to interpolation/extrapolation of gridcell-averaged b_w in different ways for LR and OK. LR interpolation uncertainty is represented by a multivariate normal distribution of possible regression coefficients (β). The standard deviation of each distribution is calculated using the covariance of β as outlined in Bagos and Adam (2015), which ensures that the β values are internally consistent. The β distributions are randomly sampled and used to calculate gridcell-estimated b_w.

OK interpolation uncertainty is represented by the standard deviation for each gridcell-estimated value of b_w generated by the DiceKriging package. The standard deviation of B_w is then found by taking the square root of the average variance of each gridcell-estimated b_w. The final distribution of B_w values is centred at the B_w estimated with OK. For simplicity, the standard deviation of B_w values that results from

either LR or OK interpolation/extrapolation uncertainty is referred to as σ_{INT}.

4. RESULTS

4.1. Field measurements

4.1.1. Snow depth
Mean snow depth varied systematically across the study region, with Glacier 4 having the highest mean snow depth and Glacier 13 having the lowest (Fig. 2a). At each measurement location, the median range of measured depths (3–4 points) as a percent of the mean local depth is 2, 11 and 12%, for Glaciers 4, 2 and 13, respectively. While Glacier 4 has the lowest point-scale variability, as assessed above, it also has the highest proportion of outliers, indicating a more variable snow depth across the glacier. The average standard deviation of all zigzag depth measurements is
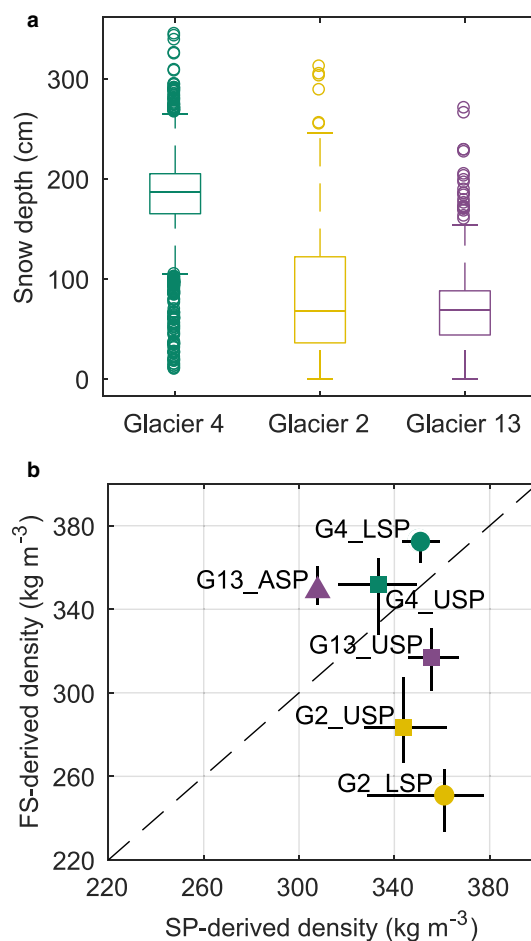

Fig. 2. Measured snow depth and density. (a) Boxplot of measured snow depth on Glaciers 4, 2 and 13 with the first quartiles (box), median (line within box), minimum and maximum values excluding outliers (bar) and outliers (circles), which are defined as being outside of the range of 1.5 times the quartiles ($\sim\pm 2.7\sigma$). (b) Comparison of depth-averaged densities estimated using Federal Sampler (FS) measurements and a wedge cutter in a snow pit (SP) for Glacier 4 (G4), Glacier 2 (G2) and Glacier 13 (G13). Labels indicate SP locations in the accumulation area (ASP), upper ablation area (USP) and lower ablation area (LSP). Error bars for SP-derived densities are calculated by varying the thickness and density of layers that are too hard to sample, and error bars for FS-derived densities are the standard deviation of measurements taken at one location. One-to-one line is dashed.
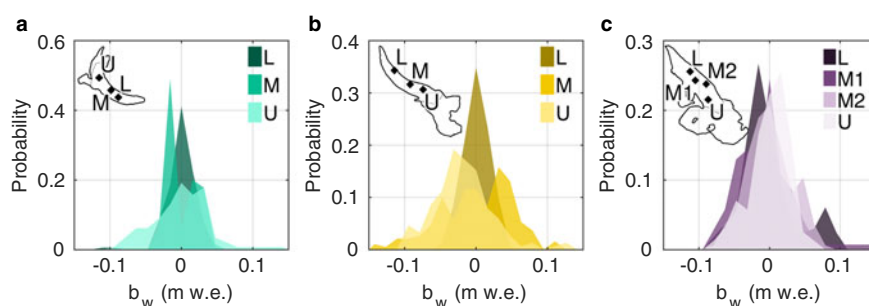
Fig. 3. Distributions of estimated winter-balance values for each zigzag survey in lower (L), middle (M) and upper (U) ablation areas (insets). Local mean has been subtracted. (a) Glacier 4. (b) Glacier 2. (c) Glacier 13.

0.07, 0.17 and 0.14 m, for Glaciers 4, 2 and 13, respectively. When converted to values of b_w using the local FS-derived density measurement, the average standard deviation is 0.027 m w.e., 0.035 m w.e. and 0.040 m w.e. Winter-balance data for each zigzag are not normally distributed (Fig. 3).

4.1.2. Snow density

Contrary to expectation, co-located FS and SP measurements are found to be uncorrelated ($R^2 = 0.25$, Fig. 2b). The FS appears to oversample in deep snow and undersample in shallow snow. Oversampling by small-diameter sampling tubes has been observed in previous studies, with a percent error between 6.8 and 11.8% (e.g. Work and others, 1965; Fames and others, 1982; Conger and McClung, 2009). Studies that use FS often apply a 10% correction to all measurements for this reason (e.g. Molotch and others, 2005). Oversampling has been attributed to slots 'shaving' snow into the tube as it is rotated (e.g. Dixon and Boon, 2012) and to snow falling into the slots, particularly for snow samples with densities > 400 kg m^{-3} and snow depths > 1 m (e.g. Beaumont and Work, 1963). Undersampling is likely to occur due to loss of snow from the bottom of the sampler (Turcan and Loijens, 1975). The loss by this mechanism may have occurred in our study, given the isothermal and melt-affected snow conditions observed over the lower reaches of Glaciers 2 and 13. Relatively poor FS spring-scale sensitivity also calls into question the reliability of measurements for snow depths < 20 cm.

Our FS-derived density values are positively correlated with snow depth ($R^2 = 0.59$). This relationship could be a result of physical processes, such as compaction in deep snow and preferential formation of depth hoar in shallow snow, but is more likely a result of measurement artefacts for a number of reasons. First, the total range of densities measured by the FS seems improbably large (227–431 kg m^{-3}). At the time of sampling, the snowpack had little new snow, few ice lenses and was not saturated; the range of measured densities is, therefore, difficult to explain with physical conditions. Moreover, the range of FS-derived values is much larger than that of SP-derived values when co-located measurements are compared. Second, compaction effects of the magnitude required to explain the density differences between SP and FS measurements would not be expected at the measured snow depths (up to 340 cm). Third, no linear relationship exists between depth and SP-derived density ($R^2 = 0.05$). These findings suggest that the FS measurements have a bias for which we have not identified a suitable correction. Despite this bias, we use FS-derived

densities to generate a range of possible b_w estimates and to provide a generous estimate of uncertainty arising from density assignment.

4.2. Density assignment

Given the lack of correlation between co-located SP- and FS-derived densities (Fig. 2), we use the densities derived from these two methods separately (Table 3). SP-derived regional (S1) and glacier-mean (S2) densities are within one standard deviation of the corresponding FS-derived densities (F1 and F2) although SP-derived density values are larger (see Supplementary Material, Table S3). For both SP- and FS-derived densities, the mean density for any given glacier (S2 or F2) is within one standard deviation of the mean across all glaciers (S1 or F1). Correlations between elevation and SP- and FS-derived densities are generally high ($R^2 > 0.5$) but vary between glaciers (Supplementary Material, Table S3). For any given glacier, the standard deviation of the 3–4 SP- or FS-derived densities is <13% of the mean of those values (S2 or F2) (Supplementary Material, Table S3). We adopt S2 (glacier-wide mean of SP-derived densities) as the reference method of density assignment. Though the method described by S2 does not account for known basin-scale spatial variability in snow density (e.g. Wetlaufer and others, 2016), it is commonly used in winter-balance studies (e.g. Elder and others, 1991; McGrath and others, 2015; Cullen and others, 2017).

Table 3. Eight methods used to estimate snow density at unmeasured locations. Source of snow density values include snow pit (SP) and Federal Sampler (FS) measurements. Total number of resulting density values given in parentheses, with n_T the total number of snow-depth measurement locations along transects (Table 1)

Method code	Snow density measurement SP	Snow density measurement FS	Density assignment method
S1 F1	■	■	Mean of measurements across all glaciers (1)
S2 F2	■	■	Mean of measurements for each glacier (3)
S3 F3	■	■	Regression of density on elevation for each glacier (n_T)
S4 F4	■	■	Inverse distance weighted mean for each glacier (n_T)

4.3. Gridcell-averaged winter balance

The distributions of gridcell-averaged b_w values for the individual glaciers are similar to those in Fig. 2a but with fewer outliers (see Supplementary Material, Fig. S4). The standard deviations of b_w values determined from the zigzag surveys are almost twice as large as the mean standard deviation of point-scale b_w values within a gridcell measured along transects (see Supplementary Material, Fig. S5). However, a small number of gridcells sampled in transect surveys have standard deviations in b_w that exceed 0.25 m w.e. (~10 times greater than those for zigzag surveys).

4.4. Distributed winter balance

4.4.1. Linear regression

The highest values of estimated b_w are found in the upper portions of the accumulation areas of Glaciers 2 and 13 (Fig. 4). These areas also correspond to large values of elevation, slope and wind redistribution. Extrapolation of the positive relationship between b_w and elevation, as well as slope and Sx for Glacier 2, results in high b_w estimates and large combined uncertainty in these estimates (Fig. 5). On Glacier

4, the distributed b_w is nearly uniform (Fig. 4) due to the small regression coefficients for all topographic parameters. The variance explained by the LR-estimated b_w differs considerably between glaciers (Fig. 6), with the best correlation between modelled and observed b_w occurring for Glacier 2. LR is an especially poor predictor of b_w on Glacier 4, where B_w can be estimated equally well using the mean of the data. RMSE is also the highest for Glacier 4 (Table 4).

4.4.2. Ordinary kriging

For all three glaciers, large areas that correspond to locations far from measurements have b_w estimates equal to the kriging mean. Distributed b_w estimated with OK on Glacier 4 is mostly uniform except for local deviations close to measurement locations (Fig. 4) and combined uncertainty is high across the glacier. Distributed b_w varies more smoothly on Glaciers 2 and 13 (Fig. 4). Glacier 2 has a distinct region of low estimated b_w (~0.1 m w.e.) in the lower part of the ablation area, which corresponds to a wind-scoured region of the glacier. Glacier 13 has the lowest estimated mean b_w and only small deviations from this mean at the
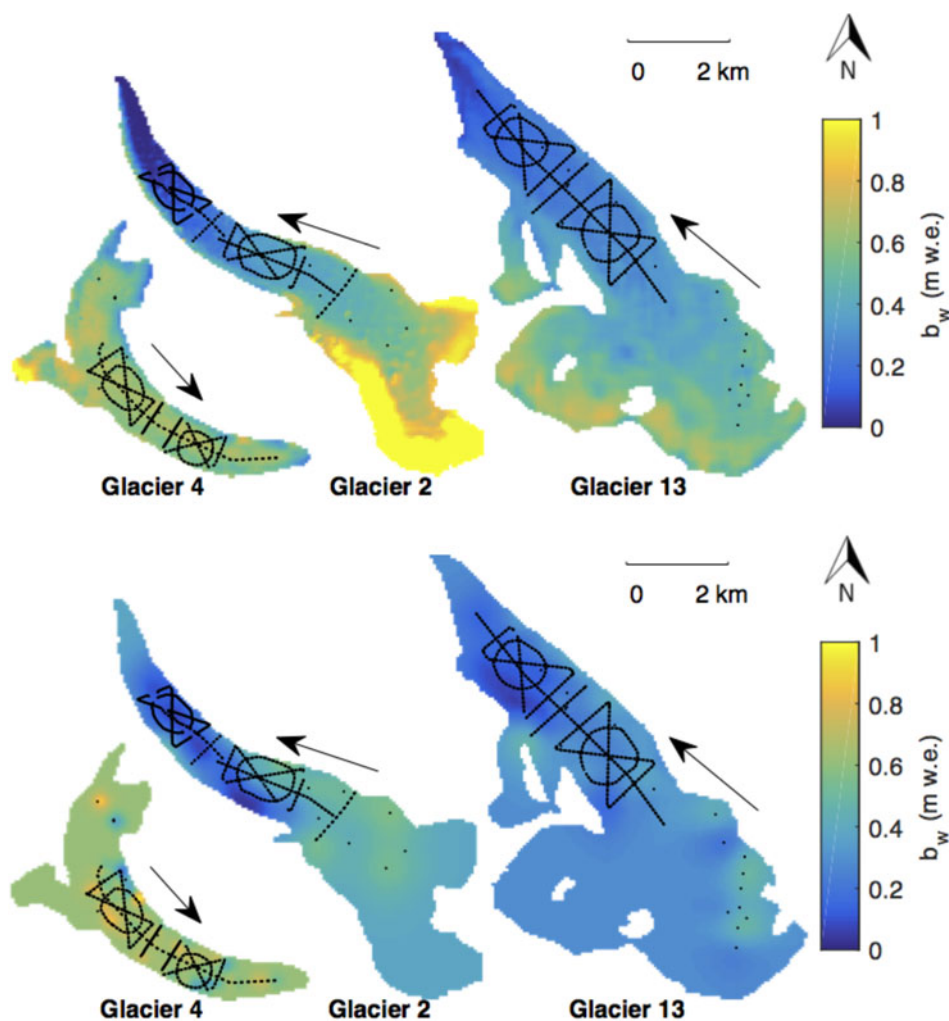

Fig. 4. Spatial distribution of winter balance (b_w) estimated using linear regression (LR) (top row) and ordinary kriging (OK) (bottom row) with densities assigned as per S2 (Table 3). The LR method involves multiplying regression coefficients, found using cross validation and model averaging, by topographic parameters for each gridcell. OK uses the correlation of measured values to find a set of optimal weights for estimating values at unmeasured locations. Locations of snow-depth measurements made in May 2016 are shown as black dots. Ice-flow directions are indicated by arrows.
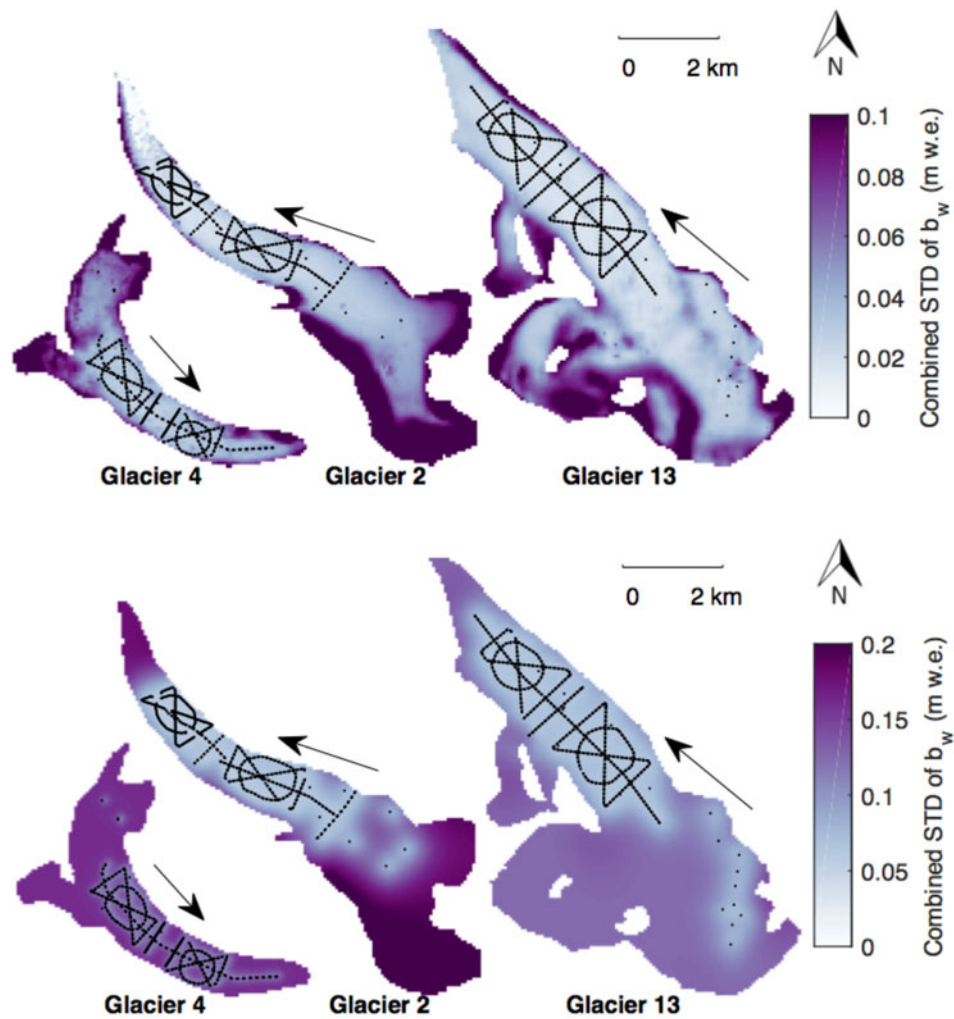
Fig. 5. Combined uncertainty of distributed winter balance (b_w) for density-assignment method S2 (Fig. 4) found using linear regression (top row) and ordinary kriging (bottom row). Ice flow directions are indicated by arrows.

measurement locations (Fig. 4). Combined uncertainty varies considerably across the three study glaciers with the greatest uncertainty far from measurement locations

(Fig. 5). The variance explained by OK-estimated b_w is high for Glaciers 2 and 13 relative to that for Glacier 4 (Fig. 6).
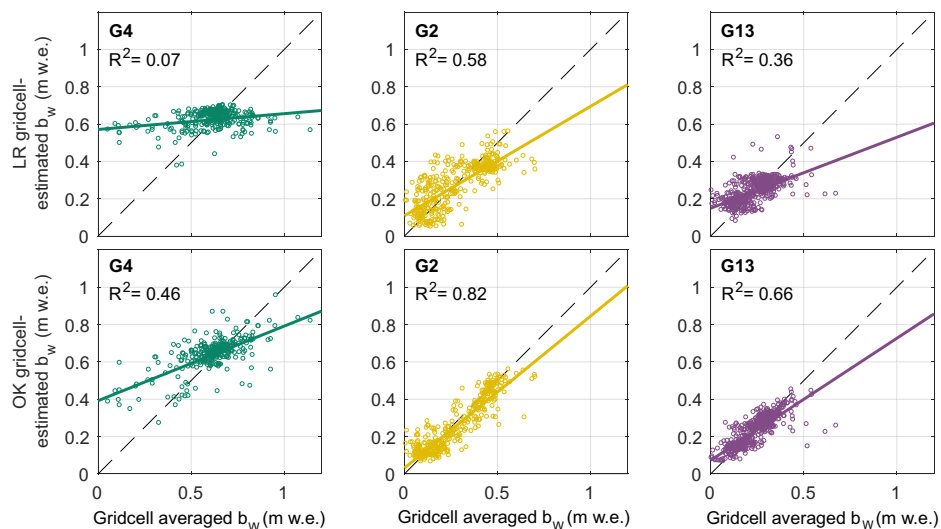
Fig. 6. Winter balance (b_w) estimated by linear regression (LR, top row) or ordinary kriging (OK, bottom row) versus the gridcell-averaged b_w data for Glacier 4 (left), Glacier 2 (middle) and Glacier 13 (right). Each circle represents a single gridcell. Explained variance (R^2) is provided. Best-fit (solid) and one-to-one (dashed) lines are shown.

Table 4. Glacier-wide winter balance (B_w, m w.e.) estimated using linear regression and ordinary kriging for the three study glaciers (S2 density method). RMSE (m w.e.) is computed between gridcell-averaged values of b_w (the data) that were randomly selected and excluded from interpolation ($\sim 1/3$ of all data) and those estimated by interpolation. RMSE as a percent of B_w is shown in parentheses

	Linear regression		Ordinary kriging	
	B_w	RMSE	B_w	RMSE
G4	0.60	0.15 (25%)	0.62	0.12 (19%)
G2	0.52	0.10 (19%)	0.34	0.07 (21%)
G13	0.39	0.08 (21%)	0.28	0.06 (21%)

4.5. Uncertainty analysis using a Monte Carlo approach

Estimates of B_w are affected by uncertainty introduced by the representativeness of gridcell-averaged values of b_w (σ_{GS}), choosing a method of density assignment (σ_ρ), and interpolating/extrapolating b_w values across the domain (σ_{INT}). Using a Monte Carlo analysis, we find that interpolation uncertainty contributes more to B_w uncertainty than grid-scale uncertainty or the method of density assignment (see Supplementary Material). In other words, the distribution of B_w that arises from grid-scale uncertainty and the differences in distributions of B_w due to different methods of density assignment are generally smaller than the distribution that arises from interpolation uncertainty (Fig. 7 and Table 5). B_w distributions obtained using LR are strongly affected by extrapolation of positive linear relationships into the upper portion of the accumulation area. OK-estimated values of b_w in the accumulation area are generally uniform (Fig. 4) but are sensitive to small variations in gridcell-averaged b_w at locations along the edge of the survey. As a result, the uncertainty in OK-estimated values of B_w is large, and unrealistic values (e.g. $B_w = 0$ m w.e.) are possible (Fig. 7).

The values of B_w for our study glaciers (using LR and the S2 density assignment), with an uncertainty equal to one standard deviation of the distribution found with Monte Carlo analysis, are: 0.60 ± 0.03 m w.e. for Glacier 4, 0.52 ± 0.05 m w.e. for Glacier 2 and 0.39 ± 0.03 m w.e. for Glacier 13. The B_w uncertainty from the three investigated sources of uncertainty ranges from 0.03 to 0.05 m w.e. (5–9%) for LR estimates and from 0.10 to 0.15 m w.e. (24–39%) for OK estimates.

5. DISCUSSION

5.1. Distributed winter balance

5.1.1. Linear regression

Of the topographic parameters in the LR, elevation (z) is the most significant predictor of gridcell-averaged b_w for Glaciers 2 and 13, while wind redistribution (Sx) is the most significant predictor for Glacier 4 (Fig. 8). As expected, gridcell-averaged b_w is positively correlated with elevation where the correlation is significant. It is possible that the elevation correlation was accentuated due to melt onset for Glacier 13 in particular. Glacier 2 had little snow at the terminus likely due to steep slopes and wind-scouring but the snow did not appear to have been affected by melt. Our results are consistent with many studies that have found elevation to be the most significant predictor of seasonal snow accumulation data (e.g. Machguth and others, 2006; Grünewald and others, 2014; McGrath and others, 2015). The b_w–elevation gradient is 13 mm w.e. 100 m^{-1} on Glacier 2 and 7 mm w.e. 100 m^{-1} on Glacier 13. These gradients are consistent with those reported for a few glaciers in Svalbard (Winther and others, 1998) but are considerably lower than many reported b_w–elevation gradients, which range from $\sim$60 to 240 mm w.e. 100 m^{-1} (e.g. Hagen and Liestøl, 1990; Tveit and Killingtveit, 1994; Winther and others, 1998). Extrapolating linear relationships to unmeasured locations typically results in considerable estimation error, as seen by the large b_w values (Fig. 4) and large combined uncertainty (Fig. 5) in the high-elevation regions of
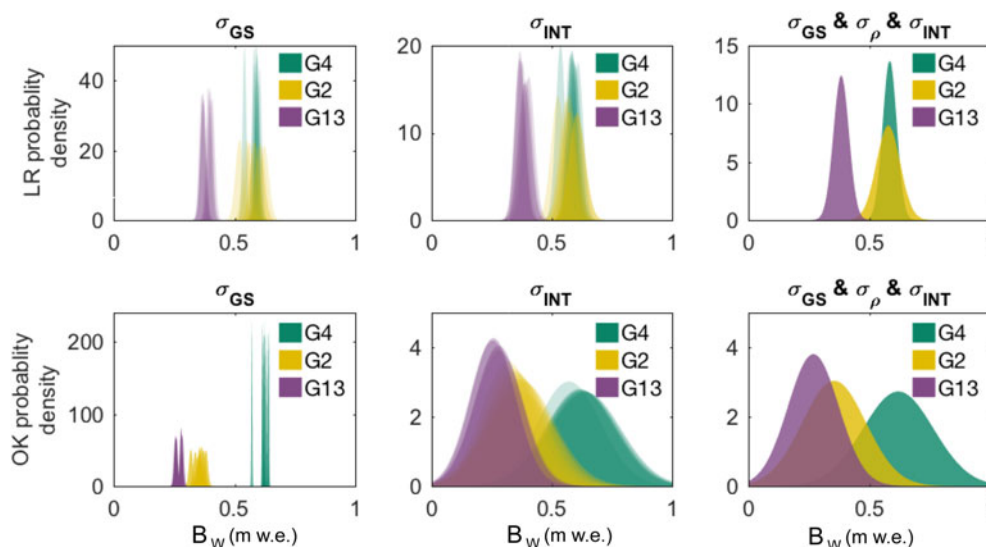

Fig. 7. Distributions of glacier-wide winter balance (B_w) for Glaciers 4 (G4), 2 (G2) and 13 (G13) that arise from various sources of uncertainty. B_w distribution arising from grid-scale uncertainty (σ_{GS}) (left column). B_w distribution arising from interpolation uncertainty (σ_{INT}) (middle column). B_w distribution arising from a combination of σ_{GS}, σ_{INT} and density assignment uncertainty (σ_ρ) (right column). Results are shown for interpolation by linear regression (LR, top row) and ordinary kriging (OK, bottom row). Left two columns include eight distributions per glacier (colour) and each corresponds to a density assignment method (S1–S4 and F1–F4).

Table 5. Standard deviation ($\times 10^{-2}$ m w.e.) of glacier-wide winter balance (B_w) distributions arising from uncertainties in grid-scale b_w (σ_{GS}), density assignment (σ_ρ), interpolation (σ_{INT}) and all three sources combined (σ_{ALL}) for linear regression (left columns) and ordinary kriging (right columns)

	Linear regression				Ordinary kriging			
	σ_{GS}	σ_ρ	σ_{INT}	σ_{ALL}	σ_{GS}	σ_ρ	σ_{INT}	σ_{ALL}
Glacier 4	0.86	1.90	2.13	2.90	0.18	2.16	14.35	14.64
Glacier 2	1.80	3.37	3.09	4.90	0.80	2.06	12.65	13.14
Glacier 13	1.12	1.68	2.80	3.20	0.57	1.30	9.74	10.48

Glaciers 2 and 13. The low correlation between b_w and elevation on Glacier 4 is consistent with Grabiec and others (2011) and López-Moreno and others (2011), who conclude that highly variable distributions of snow can be attributed to complex interactions between topography and the atmosphere that cannot be easily quantified. The snow on Glacier 4 also did not appear to have been affected by melt and it is hypothesized that significant wind-redistribution of snow, which was not captured by the Sx parameter, obscured ice topography and produced a relatively uniform snow depth across the glacier.

Gridcell-averaged b_w is negatively correlated with Sx on Glacier 4, counter-intuitively indicating less snow in what would be interpreted as sheltered areas. Gridcell-averaged b_w is positively correlated with Sx on Glaciers 2 and 13. Our results corroborate those of McGrath and others (2015) in a study of six glaciers in Alaska (DEM resolutions of 5 m)
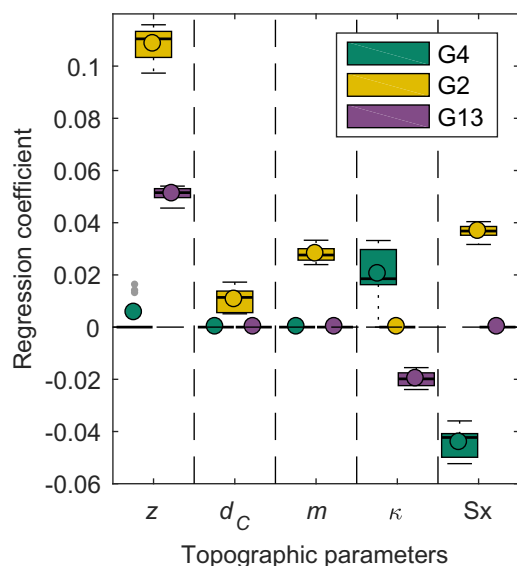

Fig. 8. Distribution of coefficients (β) determined by linear regression of gridcell-averaged b_w on DEM-derived topographic parameters for the eight different density assignment methods (Table 3). Coefficients are calculated using standardized data, so values can be compared across parameters. Regression coefficients that are not significant are assigned a value of zero. Topographic parameters include elevation (z), distance from centreline (d_C), slope (m), curvature (κ) and wind redistribution (Sx). Aspect and 'northness' are not shown because coefficient values are zero in every case. The box plot shows first quartiles (box), median (line within box), mean (circle within box), minimum and maximum values excluding outliers (bars) and outliers (gray dots), which are defined as being outside of the range of 1.5 times the quartiles ($\sim\pm 2.7\sigma$).

where elevation and Sx were the only significant parameters for all glaciers; Sx regression coefficients were smaller than elevation regression coefficients, and in some cases, negative. While our results point to wind having an impact on snow distribution, the wind redistribution parameter (Sx) may not adequately capture these effects at our study sites. For example, Glacier 4 has a curvilinear plan-view profile and is surrounded by steep valley walls, so specifying a single cardinal direction for wind may not be adequate. Further, the scale of deposition may be smaller than the resolution of the Sx parameter estimated from the DEM. Creation of a parametrization for sublimation from blowing snow, which has been shown to be an important mechanism of mass loss from ridges (e.g. Musselman and others, 2015), may also increase the explanatory power of LR for our study sites.

We find that transfer of LR coefficients between glaciers results in large estimation errors. Regression coefficients from Glacier 4 produce the highest RMSE (0.38 m w.e. on Glacier 2 and 0.40 m w.e. on Glacier 13, see Table 4 for comparison) and B_w values are the same for all glaciers (0.64 m w.e.) due to the dominance of the regression intercept. Even if the LR is performed with b_w values from all glaciers combined, the resulting coefficients produce large RMSE when applied to individual glaciers (0.31 m w.e., 0.15 m w.e. and 0.14 m w.e. for Glaciers 4, 2 and 13, respectively). Our results are consistent with those of Grünewald and others (2013), who found that local statistical models cannot be transferred across basins and that regional-scale models are not able to explain the majority of observed variance in winter balance.

5.1.2. Ordinary kriging

Due to a paucity of data, OK produces almost uniform gridcell-estimated b_w in the accumulation area of each glacier, inconsistent with observations described in the literature (e.g. Machguth and others, 2006; Grabiec and others, 2011). Glacier 4 has the highest estimated mean with large deviations from the mean at measurement locations. The longer correlation lengths of the data for Glaciers 2 and 13 result in a more smoothly varying distributed b_w. As expected, extrapolation using OK leads to large uncertainty (Fig. 5), further emphasizing the need for spatially distributed point-scale measurements.

5.1.3. Sensitivity of winter balance to interpolation/ extrapolation method

The physically-based LR estimates and the statistically-based OK estimates result in different distributions of b_w for the three study glaciers (Fig. 4). Since LR is based on physical parameters, extrapolation to areas with extreme values of

these parameters can lead to sharp changes in estimated b_w and to large uncertainty (Fig. 7), due to the sensitivity of the regression to each topographic parameter. The accumulation areas of Glaciers 2 and 13 have large estimated b_w values because observations are sparse and topographic parameters, such as elevation, attain their highest values.

In contrast, OK tends to result in extrapolated values of b_w that approach the data mean and are smoothly varying. For Glaciers 2 and 13, OK estimates are more than ~0.22 m w.e. (39%) and ~0.11 m w.e. (30%) lower than LR estimates, respectively (Table 4). The influence of elevation results in substantially higher LR-estimated values of b_w at high elevation, whereas OK-estimated values are more uniform. Since OK is a data-fitting interpolation method, the absolute RMSE of OK is ~0.03 m w.e. lower for all glaciers (Table 4).

These two different methods produce similar estimates of distributed b_w (Fig. 4) and B_w (~0.6 m w.e., Table 4) on Glacier 4, but both are relatively poor predictors of b_w in measured gridcells (Fig. 6). Additionally, RMSEs as a percentage of glacier-wide B_w are comparable between LR and OK (Table 4) with an average RMSE of 21%. This comparability is interesting, given that all of the data were used to generate the OK model, while only ~2/3 were used in the LR. Tests in which only ~2/3 of the data were used in the OK model yielded similar results to those in which all data were used.

5.2. Uncertainty analysis using a Monte Carlo approach

Interpolation/extrapolation of b_w data is the largest contributor to b_w uncertainty in our study. These results caution strongly against including interpolated/extrapolated values of b_w in comparisons with remote sensing- or model-derived estimates of b_w. If possible, such comparisons should be restricted to point-scale data. Grid-scale uncertainty (σ_{GS}) is the smallest assessed contributor to overall B_w uncertainty. This result is consistent with the generally smoothly-varying snow depths encountered in zigzag surveys, and previously reported ice-roughness lengths on the order of centimetres (e.g. Hock, 2005) compared with snow depths on the order of decimetres to metres. Given our assumption that zigzags are an adequate representation of grid-scale variability, the low B_w uncertainty arising from σ_{GS} implies that subgrid-scale sampling need not be a high priority for reducing overall uncertainty. Our assumption that the 3–4 zigzag surveys can be used to estimate glacier-wide σ_{GS} may be flawed, particularly in areas with debris cover, crevasses and steep slopes.

Our analysis did not include uncertainty arising from density measurement errors associated with the FS, wedge cutters and spring scales, from vertical and horizontal errors in the DEM or from the error associated with estimating measurement locations based on the GPS position of the lead observer. We assume that these sources of uncertainty are either encompassed by the sources investigated or are negligible.

5.3. Regional winter-balance gradient

Although we find considerable inter- and intra-basin variability in winter balance, our results are consistent with a regional-scale winter-balance gradient for the continental side of the St. Elias Mountains (Fig. 9). Winter-balance data

are compiled from Taylor-Barge (1969), the three glaciers presented in this paper and two snow pits we analyzed near the head of the Kaskawulsh Glacier between 20 and 21 May 2016. The data show a linear decrease of 0.024 m w.e. km^{-1} ($R^2 = 0.85$) in winter balance with distance from the regional topographic divide between the Kaskawulsh and Hubbard Glaciers, as identified by Taylor-Barge (1969). While the three study glaciers fit the regional trend, the same relationship would not apply if just the Donjek Range were considered. We hypothesize that interaction between meso-scale weather patterns and large-scale mountain topography is a major driver of regional-scale winter balance. Further insight into regional-scale patterns of winter balance in the St. Elias Mountains could be gained by investigating moisture source trajectories and the contribution of orographic precipitation.

5.4. Limitations and future work

The potential limitations of our work include the restriction of our data to a single year, minimal sampling in the accumulation area, the problem of uncorrelated SP- and FS-derived densities, a sampling design that could not be optimized a priori, the assumption of spatially uniform subgrid variability and lack of more finely resolved DEMs.

Interannual variability in winter balance is not considered in our study. A number of studies have found temporal stability in spatial patterns of snow distribution and that statistical models based on topographic parameters could be applied reliably between years (e.g. Grünewald and others, 2013). For example, Walmsley (2015) analyzed more than 40 years of winter balance recorded on two Norwegian glaciers and found that snow distribution is spatially heterogeneous yet
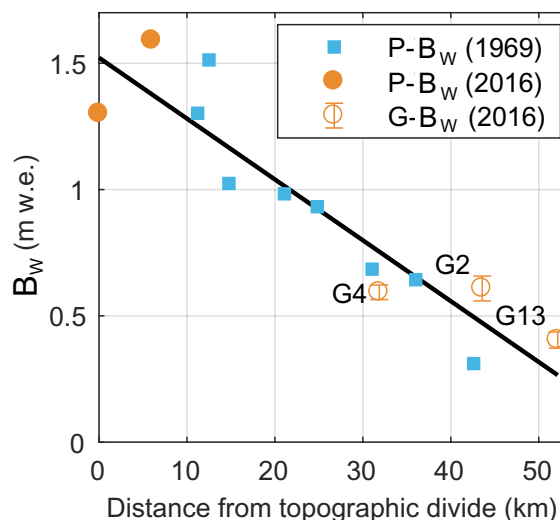

Fig. 9. Relationship between winter balance (B_w) and linear distance from the regional topographic divide between the Kaskawulsh and Hubbard Glaciers in the St. Elias Mountains. Point-scale values of winter balance from snow-pit data reported by Taylor-Barge (1969) (blue boxes, P-B_w). LR-estimated B_w calculated using density assignment S2 for Glaciers 4 (G4), 2 (G2) and 13 (G13) with errors bars calculated as the standard deviation of Monte Carlo-derived B_w distributions (this study) (open orange circles, G-B_w). Point-scale B_w estimated from snow-pit data at two locations in the accumulation area of the Kaskawulsh Glacier, collected in May 2016 (unpublished data, SFU Glaciology Group) (filled orange dots, P-B_w). Black line indicates best fit ($R^2 = 0.85$).

exhibits robust temporal stability. Contrary to this, Crochet and others ([2007](#)) found that snow distribution in Iceland differed considerably between years and depended primarily on the dominant wind direction over the course of a winter. Therefore, multiple years of snow depth and density measurements are needed to better understand interannual variability of winter balance within the Donjek Range.

There is a conspicuous lack of data in the accumulation areas of our study glaciers. With increased sampling in the accumulation area, interpolation uncertainties would be reduced where they are currently greatest and the LR would be better constrained. Although certain regions of the glaciers remain inaccessible for direct measurements, other methods of obtaining winter-balance measurements, including ground-penetrating radar and DEM differencing with photogrammetry or lidar, could be used in conjunction with manual probing to increase the spatial coverage of measurements.

The lack of correlation between SP- and FS-derived densities needs to be reconciled. Contrary to our results, most studies that compare SP- and FS-derived densities report minimal discrepancy (e.g. Dixon and Boon, [2012](#), and sources within). Additional co-located density measurements are needed to better compare the two methods of obtaining density values. Comparison with other FS would also be informative. Even with this limitation, density assignment was, fortunately, not the largest source of uncertainty in estimating glacier-wide winter balance.

Our sampling design was chosen to achieve broad spatial coverage of the ablation area, but is likely too finely resolved along transects for many mass-balance surveys to replicate. An optimal sampling design would minimize uncertainty in winter balance while reducing the number of required measurements. Analysis of the estimated winter balance obtained using subsets of the data is underway to make recommendations on optimal transect configuration and along-track spacing of measurements. López-Moreno and others ([2010](#)) found that 200–400 observations are needed within a non-glacierized alpine basin (6 km^2) to obtain accurate and robust snow distribution models. Similar guidelines would be useful for glacierized environments.

In this study, we assume that the subgrid variability of winter balance is uniform across a given glacier. Contrary to this assumption, McGrath and others ([2015](#)) found greater variability of winter-balance values close to the terminus. Testing our assumption could be a simple matter of prioritizing the labour-intensive zigzags surveys. To ensure consistent quantification of subgrid variability, zigzag survey measurements could also be tested against other measurements methods, such as lidar.

DEM gridcell size is known to influence values of computed topographic parameters (Zhang and Montgomery, [1994](#); Garbrecht and Martz, [1994](#); Guo-an and others, [2001](#); López-Moreno and others, [2010](#)). The relationship between topographic parameters and winter balance is, therefore, not independent of DEM gridcell size. For example, Kienzle ([2004](#)) and López-Moreno and others ([2010](#)) found that a decrease in spatial resolution of the DEM results in a decrease in the importance of curvature and an increase in the importance of elevation in LR of snow distribution on topographic parameters in non-glacierized basins. The importance of curvature in our study is affected by the DEM smoothing that we applied to obtain a spatially continuous curvature field (see Supplementary Material, Fig. S1). A comparison of regression coefficients from high-resolution DEMs obtained from various sources and sampled with various gridcell sizes could be used to characterize the dependence of topographic parameters on DEMs, and therefore assess the robustness of inferred relationships between winter balance and topographic parameters.

6. CONCLUSION

We estimate winter balance for three glaciers (termed Glacier 2, Glacier 4 and Glacier 13) in the St. Elias Mountains, Yukon, Canada from multiscale snow depth and density measurements. Linear regression and ordinary kriging are used to obtain estimates of distributed winter balance (b_w). We use Monte Carlo analysis to evaluate the contributions of interpolation, assignment of snow density and grid-scale variability of winter balance to uncertainty in estimates of glacier-wide winter balance (B_w).

Values of B_w estimated using LR and OK differ by up to 0.18 m w.e. We find that interpolation uncertainty is the largest assessed source of uncertainty in B_w (5–9% for LR estimates and 24–39% for OK estimates). Uncertainty resulting from the method of density assignment is comparatively low, despite the wide range of methods explored. Given our representation of grid-scale variability, the resulting B_w uncertainty is small indicating that extensive subgrid-scale sampling is not required to reduce overall uncertainty.

Our results suggest that processes governing distributed b_w differ between glaciers, highlighting the importance of regional-scale winter-balance studies. On Glacier 4, measured values of b_w are characterized by high variability with many outliers, leading to poor correlation with estimated values. Measured values on Glacier 2 and 13 were less variable, with elevation being a significant predictor of gridcell-averaged b_w. A wind-redistribution parameter is found to be a weak but significant predictor of b_w, though conflicting relationships between glaciers make it difficult to interpret. The major limitations of our work include the restriction of our data to a single year and minimal sampling in the accumulation area. Although challenges persist when estimating winter balance, our data are consistent with a regional-scale winter-balance gradient for the continental side of the St. Elias Mountains.

7. AUTHOR CONTRIBUTION STATEMENT

AP planned and executed the data collection, performed all calculations and analysis and drafted and edited the manuscript. GF conceived of the study, contributed to field planning and data collection, oversaw all stages of the work and edited the manuscript. VR provided guidance on the methods of data analysis and edited the manuscript. DB provided insight into the statistical analysis and edited the manuscript.

SUPPLEMENTARY MATERIAL

The supplementary material for this article can be found at https://doi.org/10.1017/jog.2018.68

ACKNOWLEDGMENTS

REFERENCES

Anderton SP, White SM and Alvera B (2004) Evaluation of spatial variability in snow water equivalent for a high mountain catchment. *Hydrol. Process.*, **18**(3), 435–453

Arendt AA and 5 others (2008) Validation of high-resolution GRACE mascon estimates of glacier mass changes in the St Elias Mountains, Alaska, USA, using aircraft laser altimetry. *J. Glaciol.*, **54**(188), 778–787

Bagos PG and Adam M (2015) On the covariance of regression coefficients. *Open J. Stat.*, **5**, 680–701

Balk B and Elder K (2000) Combining binary decision tree and geostatistical methods to estimate snow distribution in a mountain watershed. *Water Resour. Res.*, **36**(1), 13–26

Barry RG (1992) *Mountain weather and climate*, 3rd edn. Cambridge University Press

Beaumont RT and Work RA (1963) Snow sampling results from three samplers

Berthier E, Schiefer E, Clarke GKC, Menounos B and Rémy F (2010) Contribution of Alaskan glaciers to sea-level rise derived from satellite imagery. *Nat. Geosci.*, **3**(2), 92–95

Burgess EW, Forster RR and Larsen CF (2013) Flow velocities of Alaskan glaciers. *Nat. Commun.*, **4**, 2146–2154

Burnham KP and Anderson DR (2004) Multimodel inference: understanding AIC and BIC in model selection. *Sociol. Method. Res.*, **33**(2), 261–304

Carroll T (1977) A comparison of the CRREL 500 cm^3 tube and the ILTS 200 and 100 cm^3 box cutters used for determining snow densities. *J. Glaciol.*, **18**(79), 334–337

Clark MP and 8 others (2011) Representing spatial variability of snow water equivalent in hydrologic and land-surface models: a review. *Water Resour. Res.*, **47**(7)

Clarke GKC (2014) A short and somewhat personal history of Yukon glacier studies in the Twentieth Century. *Arctic*, **37**(1), 1–21

Clyde GD (1932) Circular No. 99-Utah Snow Sampler and Scales for Measuring Water Content of Snow. *UAES Circulars*, Paper 90

Cogley JG and 9 others (2011) *Glossary of glacier mass balance and related terms*. UNESCO-IHP, Paris

Conger SM and DM McClung (2009) Comparison of density cutters for snow profile observations. *J. Glaciol.*, **55**(189), 163–169

Crochet P and 6 others (2007) Estimating the spatial distribution of precipitation in iceland using a linear model of orographic precipitation. *J. Hydrometeorol.*, **8**(6), 1285–1306

Crompton JW and Flowers GE (2016) Correlations of suspended sediment size with bedrock lithology and glacier dynamics. *Ann. Glaciol.*, **57**(72), 1–9

Cullen NJ and 10 others (2017) An 11-year record of mass balance of Brewster Glacier, New Zealand, determined using a geostatistical approach. *J. Glaciol.*, **63**(238), 199–217

Dadić R, Mott R, Lehning M and Burlando P (2010) Parameterization for wind-induced preferential deposition of snow. *J. Geophys. Res.-Earth*, **24**(14), 1994–2006

Danby RK, Hik DS, Slocombe DS and Williams A (2003) Science and the St. Elias: an evolving framework for sustainability in North America's highest mountains. *Geogr. J.*, **169**(3), 191–204

Davis JC and Sampson RJ (1986) *Statistics and data analysis in geology*, 2nd edn. Wiley, New York

Deems JS and Painter TH (2006) Lidar measurement of snow depth: accuracy and error sources, *ed. Proceedings of the International Snow Science Workshop, 1-6 October, 2006, Telluride, Colorado*, Telluride, CO, International Snow Science Workshop, 30–38

Dixon D and Boon S (2012) Comparison of the SnowHydro snow sampler with existing snow tube designs. *Hydrol. Process.*, **26**(17), 2555–2562

Egli L, Griessinger N and Jonas T (2011) Seasonal development of spatial snow-depth variability across different scales in the Swiss Alps. *Ann. Glaciol.*, **52**(58), 216–222

Elder K, Dozier J and Michaelsen J (1991) Snow accumulation and distribution in an alpine watershed. *Water Resour. Res.*, **27**(7), 1541–1552

Elder K, Rosenthal W and Davis RE (1998) Estimating the spatial distribution of snow water equivalence in a montane watershed. *Hydrol. Process.*, **12**(1011), 1793–1808

Erxleben J, Elder K and Davis R (2002) Comparison of spatial interpolation methods for estimating snow distribution in the Colorado Rocky Mountains. *Hydrol. Process.*, **16**(18), 3627–3649

Fames PE, Peterson NR, Goodison BE and Richards RP (1982) Metrication of Manual Snow Sampling Equipment, Proceedings of the 50th Western Snow Conference, 120–132

Fierz CRLA and 8 others (2009) The international classification for seasonal snow on the ground, UNESCO/IHP, unesco/ihp paris ed

Garbrecht J and Martz L (1994) Grid size dependency of parameters extracted from digital elevation models. *Comput. Geosci.*, **20**(1), 85–87

Grabiec M, Puczko D, Budzik T and Gajek G (2011) Snow distribution patterns on Svalbard glaciers derived from radio-echo soundings. *Pol. Polar Res.*, **32**(4), 393–421

Gray DM and Male DH (1981) *Handbook of snow: principles, processes, management & use*, 1st edn. Pergamon Press

Grünewald T, Bühler Y and Lehning M (2014) Elevation dependency of mountain snow depth. *Cryosphere*, **8**(6), 2381–2394

Grünewald T, Schirmer M, Mott R and Lehning M (2010) Spatial and temporal variability of snow depth and ablation rates in a small mountain catchment. *Cryosphere*, **4**(2), 215–225

Grünewald T and 9 others (2013) Statistical modelling of the snow depth distribution in open alpine terrain. *Hydrol. Earth Syst. Sc.*, **17**(8), 3005–3021

Guo-an T, Yang-he H, Strobl J and Wang-qing L (2001) The impact of resolution on the accuracy of hydrologic data derived from DEMs. *J. Geogr. Sci.*, **11**(4), 393–401

Gusmeroli A, Wolken GJ and Arendt AA (2014) Helicopter-borne radar imaging of snow cover on and around glaciers in Alaska. *Ann. Glaciol.*, **55**(67), 78–88

Hagen JO and Liestøl O (1990) Long-term glacier mass-balance investigations in Svalbard, 1950–88. *Ann. Glaciol.*, **14**(1), 102–106

Helbig N and van Herwijnen A (2017) Subgrid parameterization for snow depth over mountainous terrain from flat field snow depth. *Water Resour. Res.*, **53**(2), 1444–1456

Hock R (2005) Glacier melt: a review of processes and their modelling. *Prog. Phys. Geog.*, **29**(3), 362–391

Hock R and Jensen H (1999) Application of kriging interpolation for glacier mass balance computations. *Geogr. Ann. A*, **81**(4), 611–619

Kaser G, Fountain A and Jansson P (2003) *A manual for monitoring the mass balance of mountain glaciers*. ICSI/UNESCO.

Kienzle S (2004) The effect of DEM raster resolution on first order, second order and compound terrain derivatives. *T. GIS*, **8**(1), 83–111

Kinar NJ and Pomeroy JW (2015) Measurement of the physical properties of the snowpack. *Rev. Geophys.*, **53**(2), 481–544

Kohavi R (1995) A study of cross-validation and bootstrap for accuracy estimation and model selection, Proceedings of the Fourteenth International Joint Conference on Artificial Intelligence, 1137–1145

Korona J, Berthier E, Bernard M, Rémy F and Thouvenot E (2009) SPIRIT SPOT 5 stereoscopic survey of Polar Ice: reference images and topographies during the fourth International Polar Year (2007–2009). *J. Photogram. Rem. Sens.*, **64**(2), 204–212

Lehning M and 5 others (2006) ALPINE3D: a detailed model of mountain surface processes and its application to snow hydrology. *Hydrol. Process.*, **20**(10), 2111–2128

Li J and Heap AD (2008) A review of spatial interpolation methods for environmental scientists

Liston GE and Elder K (2006) A distributed snow-evolution modeling system (SnowModel). *J. Hydrometeorol.*, **7**(6), 1259–1276

Liston GE and Sturm M (1998) A snow-transport model for complex terrain. *J. Glaciol.*, **44**(148), 498–516

López-Moreno JI and 7 others (2013) Small scale spatial variability of snow density and depth over complex alpine terrain: Implications for estimating snow water equivalent. *Adv. Water Resour.*, **55**, 40–52

López-Moreno JI, Latron J and Lehmann A (2010) Effects of sample and grid size on the accuracy and stability of regression-based snow interpolation methods. *Hydrol. Process.*, **24**(14), 1914–1928

López-Moreno JI, Fassnacht SR, Beguería S and Latron JBP (2011) Variability of snow depth at the plot scale: implications for mean depth estimation and sampling strategies. *Cryosphere*, **5**(3), 617–629

MacDougall AH and Flowers GE (2011) Spatial and temporal transferability of a distributed energy-balance glacier melt model. *J. Climate*, **24**(5), 1480–1498

Machguth H, Eisen O, Paul F and Hoelzle M (2006) Strong spatial variability of snow accumulation observed with helicopter-borne GPR on two adjacent alpine glaciers. *Geophys. Res. Lett.*, **33**(13), 1–5

Madigan D and Raftery AE (1994) Model selection and accounting for model uncertainty in graphical models using occam's window. *J. Am. Stat. Assoc.*, **89**(428), 1535–1546

Marshall HP and 7 others (2006) Spatial variability of the snowpack: Experiences with measurements at a wide range of length scales with several different high precision instruments, Proceedings International Snow Science Workshop, 359–364

McGrath D and 7 others (2015) End-of-winter snow depth variability on glaciers in Alaska. *J. Geophys. Res.-Earth*, **120**(8), 1530–1550

Metropolis N and Ulam S (1949) The Monte Carlo method. *J. Am. Stat. Assoc.*, **44**(247), 335–341

Molotch NP, Colee MT, Bales RC and Dozier J (2005) Estimating the spatial distribution of snow water equivalent in an alpine basin using binary regression tree models: the impact of digital elevation data and independent variable selection. *Hydrol. Process.*, **19**(7), 1459–1479

Mott R and 7 others (2008) Simulation of seasonal snow-cover distribution for glacierized sites on Sonnblick, Austria, with the Alpine3D model. *Ann. Glaciol.*, **49**(1), 155–160

Musselman KN, Pomeroy JW, Essery RLH and Leroux N (2015) Impact of windflow calculations on simulations of alpine snow accumulation, redistribution and ablation. *Hydrol. Process.*, **29**(18), 3983–3999

Proksch M, Rutter N, Fierz C and Schneebeli M (2016) Intercomparison of snow density measurements: bias, precision, and vertical resolution. *Cryosphere*, **10**(1), 371–384

Pulwicki A (2017) Multi-scale investigation of winter balance on alpine glaciers, (Master's thesis, Simon Fraser University)

Rasmussen CE and Williams CKI (2006) *Gaussian processes for machine learning*. MIT press Cambridge

Réveillet M, Vincent C, Six D and Rabatel A (2016) Which empirical model is best suited to simulate glacier mass balances?. *J. Glaciol.*, **63**(237), 1–16

Roustant O, Ginsbourger D and Deville Y (2012) DiceKriging, DiceOptim: two R packages for the analysis of computer experiments by kriging-based metamodeling and optimization. *J. Stat. Softw.*, **21**, 1–55

Schneiderbauer S and Prokop A (2011) The atmospheric snow-transport model: SnowDrift3D. *J. Glaciol.*, **57**(203), 526–542

Schuler TV and 5 others (2008) Distribution of snow accumulation on the Svartisen ice cap, Norway, assessed by a model of orographic precipitation. *Hydrol. Process.*, **22**(19), 3998–4008

Scipión DE, Mott R, Lehning M, Schneebeli M and Berne A (2013) Seasonal small-scale spatial variability in alpine snowfall and snow accumulation. *Water Resour. Res.*, **49**(3), 1446–1457

Shea C and Jamieson B (2010) Star: an efficient snow point-sampling method. *Ann. Glaciol.*, **51**(54), 64–72

Sold L and 5 others (2013) Methodological approaches to infer end-of-winter snow distribution on alpine glaciers. *J. Glaciol.*, **59**(218), 1047–1059

Stein ML (1999) *Interpolation of spatial data: some theory for kriging*. Springer Science & Business Media

Tangborn WV, Krimmel RM and Meier MF (1975) A comparison of glacier mass balance by glaciological, hydrological and mapping methods, South Cascade Glacier, Washington

Taylor-Barge B (1969) The summer climate of the St. Elias Mountain region, Montreal: Arctic Institute of North America, Research Paper No. 53

Thibert E, Blanc R, Vincent C and Eckert N (2008) Glaciological and volumetric mass-balance measurements: error analysis over 51 years for Glacier de Sarennes, French Alps. *J. Glaciol.*, **54**(186), 522–532

Trujillo E and Lehning M (2015) Theoretical analysis of errors when estimating snow distribution through point measurements. *Cryosphere*, **9**(3), 1249–1264

Turcan J and Loijens HS (1975) Accuracy of snow survey data and errors in snow sampler measurements, 32nd Eastern Snow Conference

Tveit J and Killingtveit Å (1994) Snow surveys for studies of water budget on Svalbard 1991–1994, Proceedings of the 10th International Northern Research Basins Symposium and Workshop, Spitsbergen, Norway. SINTEF Report, vol. 22, A96415

Waechter A, Copland L and Herdes E (2015) Modern glacier velocities across the Icefield Ranges, St Elias Mountains, and variability at selected glaciers from 1959 to 2012. *J. Glaciol.*, **61**(228), 624–634

Walmsley APU (2015) Long-term observations of snow spatial distributions at Hellstugubreen and Gråsubreen, Norway, (Master's thesis, University of Oslo)

Wetlaufer K, Hendrikx J and Marshall L (2016) Spatial heterogeneity of snow density and its influence on snow water equivalence estimates in a large mountainous basin. *Hydrology*, **3**(3), 1–17

Wilson NJ and Flowers GE (2013) Environmental controls on the thermal structure of alpine glaciers. *Cryosphere*, **7**(1), 167–182

Wilson NJ, Flowers GE and Mingo L (2013) Comparison of thermal structure and evolution between neighboring subarctic glaciers. *J. Geophys. Res.-Earth*, **118**(3), 1443–1459

Winstral A, Elder K and Davis RE (2002) Spatial snow modeling of wind-redistributed snow using terrain-based parameters. *J. Hydrometeorol.*, **3**(5), 524–538

Winther JG, Bruland O, Sand K, Killingtveit A and Marechal D (1998) Snow accumulation distribution on Spitsbergen, Svalbard, in 1997. *Polar Res.*, **17**, 155–164

Woo M-K and Marsh P (1978) Analysis of error in the determination of snow storage for small high arctic basins. *J. Appl Meteorol.*, **17**(10), 1537–1541

Wood WA (1948) Project "Snow Cornice": the establishment of the Seward Glacial research station. *Arctic*, **1**(2), 107–112

Work RA, Stockwell HJ, Freeman TG and Beaumont RT (1965) *Accuracy of field snow surveys*. Cold Regions Research & Engineering Laboratory

Zhang W and Montgomery DR (1994) Digital elevation model grid size, landscape representation, and hydrologic simulations. *Water Resour. Res.*, **30**(4), 1019–1028